

Large-scale brain functional modularity is reflected in slow electroencephalographic rhythms across the human non-rapid eye movement sleep cycle

Enzo Tagliazucchi ^{*}, Frederic von Wegner, Astrid Morzelewski, Verena Brodbeck, Sergey Borisov, Kolja Jahnke, Helmut Laufs

Department of Neurology and Brain Imaging Center, Goethe University Frankfurt am Main, Schleusenweg 2-16, 60528 Frankfurt am Main, Germany

ARTICLE INFO

Article history:

Accepted 28 December 2012
Available online 9 January 2013

Keywords:

EEG-fMRI
Modularity
Sleep
Wakefulness
Resting state
Functional networks

ABSTRACT

Large-scale brain functional networks (measured with functional magnetic resonance imaging, fMRI) are organized into separated but interacting modules, an architecture supporting the integration of distinct dynamical processes. In this work we study how the aforementioned modular architecture changes with the progressive loss of vigilance occurring in the descent to deep sleep and we examine the relationship between the ensuing slow electroencephalographic rhythms and large-scale network modularity as measured with fMRI.

Graph theoretical methods are used to analyze functional connectivity graphs obtained from fifty-five participants at wakefulness, light and deep sleep. Network modularity (a measure of functional segregation) was found to increase during deeper sleep stages but not in light sleep. By endowing functional networks with dynamical properties, we found a direct link between increased electroencephalographic (EEG) delta power (1–4 Hz) and a breakdown of inter-modular connectivity. Both EEG slowing and increased network modularity were found to quickly decrease during awakenings from deep sleep to wakefulness, in a highly coordinated fashion. Studying the modular structure itself by means of a permutation test, we revealed different module memberships when deep sleep was compared to wakefulness. Analysis of node roles in the modular structure revealed an increase in the number of locally well-connected nodes and a decrease in the number of globally well-connected hubs, which hinders interactions between separated functional modules.

Our results reveal a well-defined sequence of changes in brain modular organization occurring during the descent to sleep and establish a close parallel between modularity alterations in large-scale functional networks (accessible through whole brain fMRI recordings) and the slowing of scalp oscillations (visible on EEG). The observed re-arrangement of connectivity might play an important role in the processes underlying loss of vigilance and sensory awareness during deep sleep.

© 2013 Elsevier Inc. All rights reserved.

Introduction

The healthy and awake human brain is organized in non-random functional architectures (Bullmore and Sporns, 2009; Sporns, 2011), with large-scale connectivity networks obtained from functional magnetic resonance imaging (fMRI) revealing small-world¹ (Achard et al., 2006; Bassett and Bullmore, 2006) and scale-free² structures (Eguíluz et al., 2005; van den Heuvel et al., 2008), resistant to localized damage and efficient at large-scale information processing

(Achard and Bullmore, 2007). These networks display modular structure with densely connected subsets which are sparsely connected between them (Meunier et al., 2009a, 2009b). Modular structure was shown to be altered by normal aging (Meunier et al., 2009b) and by pathologies, including schizophrenia (Alexander-Bloch et al., 2010; Bassett et al., 2008), chronic pain (Balenzuela et al., 2010) and Alzheimer's disease (de Haan et al., 2012). Less interconnected functional modules were recently described in cognitively impaired children with frontal lobe epilepsy (Vaessen et al., 2012).

The relationship between measures of modularity (Newman and Girvan, 2004) and the degree of vigilance throughout sleep remains an interesting issue, as well as the relationship between modular structure and brain activity recorded from other imaging modalities. Previous studies have shown a departure from the small-world regime following changes in large-scale connectivity characteristic of each sleep stage (Spoormaker et al., 2010), in fact allowing sleep staging based only on fMRI information (Tagliazucchi et al., 2012).

^{*} Corresponding author. Fax: +49 1803 5518 10612.

E-mail address: tagliazucchi.enzo@googlemail.com (E. Tagliazucchi).

¹ A network retaining a rich local connectivity structure while having large distance shortcuts which sharply decrease average distance between nodes.

² A network whose degree distribution follows a power law. Nodes on the tail of the power law have a large number of connections and are termed *hubs*.

However, these changes might neither be reflected in the modularity values nor in the modular structure. A recent study (Boly et al., 2012) computed functional clustering values for fMRI recordings obtained during wakefulness and all non-rapid eye movement (NREM) sleep stages combined together, revealing a segregation increase during NREM sleep. It is not yet clear, however, how network modularity and the associated modular structure gradually develop from wakefulness to deep sleep. It is also unclear how these modularity changes and the patterns observed in scalp EEG recordings during sleep are interrelated.

Earlier studies addressing the issue of functional connectivity during sleep have in principle demonstrated the persistence of resting state networks (RSN) (Beckmann et al., 2005; Boly et al., 2012; Horovitz et al., 2008; Larson-Prior et al., 2009), except for within RSN disconnections (Horovitz et al., 2009; Sämann et al., 2011) observed for the default mode network (DMN) (Raichle et al., 2001). EEG microstates, a possible electrophysiological correlate of RSN (Britz et al., 2010), are remarkably preserved across all NREM sleep stages (Brodtbeck et al., 2012). Thus, a discrepancy arises due to the extensive behavioral changes on the one hand and the preserved RSN on the other. We hypothesize that the re-arrangement of functional connectivity across decreasing vigilance and consciousness awareness during deep sleep is related to significant changes in brain modularity, which quantifies the integration/segregation balance in large-scale functional networks. Given that shifts in vigilance are closely paralleled by changes in EEG delta power, we expect a close relationship between the latter and network modularity, in the sense that certain vigilance transitions can be equally described by EEG spectral features or by fMRI-derived integration/segregation measures. In particular, we expect temporally comparable changes in these measures from different modalities during arousals (defined as transitions from sleep to wakefulness).

This paper is structured as follows. First, we use graph theoretical methods to study the modularity values of brain functional networks across all NREM sleep stages, as well as the dynamical evolution of modularity and EEG delta power during arousals. We then correlate spontaneous connectivity fluctuations with EEG spectral power changes and we identify the role of the affected links in the modular structure. Thereafter, we proceed to examine the modular structures themselves, using a permutation method (Alexander-Bloch et al., 2012) to identify changes in module membership across sleep stages and using functional cartography (Guimerà and Amaral, 2005) to study node roles and their relevance in the modular structure. Finally, weighted networks at the group level are introduced and the module detection algorithm is applied to them, yielding information on the conformation of different functional modules during all stages of NREM sleep.

Materials and methods

EEG-fMRI acquisition and artifact correction

EEG via a cap (modified BrainCapMR, Easycap, Herrsching, Germany) was recorded continuously during fMRI acquisition (1505 volumes of T2*-weighted echo planar images, TR/TE = 2080 ms/30 ms, matrix 64 × 64, voxel size 3 × 3 × 2 mm³, distance factor 50%; FOV 192 mm²) at 3 T (Siemens Trio, Erlangen, Germany). An optimized polysomnographic setting was employed (chin and tibial EMG, ECG, EOG recorded bipolarly [sampling rate 5 kHz, low pass filter 1 kHz] with 30 EEG channels recorded with FCz as the reference [sampling rate 5 kHz, low pass filter 250 Hz]. Pulse oxymetry and respiration were recorded via sensors from the Trio [sampling rate 50 Hz]) and MR scanner compatible devices (BrainAmp MR+, BrainAmp ExG; Brain Products, Gilching, Germany), facilitating sleep scoring during fMRI acquisition (AASM, 2007; Jahnke et al., 2011; Laufs et al., 2007a).

MRI and pulse artifact correction were performed based on the average artifact subtraction (AAS) method (Allen et al., 1998) as implemented

in Vision Analyzer2 (Brain Products, Germany) followed by objective (CBC parameters, Vision Analyzer) ICA-based rejection of residual artifact-laden components after AAS resulting in EEG with a sampling rate of 250 Hz (Jahnke et al., 2011). EEG artifacts due to motion were detected and eliminated using an ICA procedure implemented in Vision Analyzer2. Sleep stages were scored manually by an expert according to the AASM criteria (AASM, 2007).

Participants

A total of sixty-three young healthy consecutive subjects with data of sufficient quality were included in the study (written informed consent, approval by the local ethics committee, participants were reimbursed for their participation). Subjects were scanned with simultaneous EEG-fMRI in the evening after following a regular sleeping schedule. Eight subjects did not fall asleep inside the scanner and were excluded from the study, resulting in a group of fifty-five subjects who reached at least N1 sleep (thirty-six females, mean ± SD age of 23.4 ± 3.3 years). Mean sleep stage durations for these participants are shown in Table 1. The detailed sleep architecture of each participant is presented in Table S1 of the Supplementary Information.

fMRI pre-processing

Using statistical parametric mapping (SPM8, www.fil.ion.ucl.ac.uk/spm) echo planar imaging (EPI) data were realigned, normalized (MNI space) and spatially smoothed (Gaussian kernel, 8 mm³ full width at half maximum). Data were re-sampled to 4 × 4 × 4 mm resolution to facilitate removal of noise and motion regressors. Note that re-sampling introduces averaging of blood oxygen level dependent (BOLD) signals, which are nevertheless finally averaged over cortical and sub-cortical regions of interest to construct functional networks. Cardiac, respiratory (both estimated using the RETROICOR method, Glover et al., 2000) and motion-induced noise were regressed out. Data were band-pass filtered in the range 0.01–0.1 Hz (Cordes et al., 2001) using a sixth order Butterworth filter.

Network construction

The organization of large-scale functional interactions between brain areas can be described in a natural way by graph theoretical methods. These methods extract information from a representation of those interactions consisting of nodes (representing brain regions) and links between those nodes (representing functional interactions) (Bullmore and Sporns, 2009; Rubinov and Sporns, 2010; Sporns et al., 2004).

In order to construct functional connectivity networks, the scheme outlined in Fig. 1 was followed. Average BOLD time courses were first extracted from each one of 116 regions defined by an automatic anatomical labeling (AAL) atlas (Tzourio-Mazoyer et al., 2002). Sleep stage epochs lasting longer than 2 minutes were identified and the average BOLD signal corresponding to that epoch was extracted from each region. This resulted in 126 epochs of wakefulness, 114 epochs of N1 sleep, 92 epochs of N2 sleep and 36 epochs of N3 sleep. Then, for

Table 1
Mean ± SD duration of contiguous sleep epochs (> 2 min) by stage.

Sleep stage	Length (min)
Wakefulness	10.29 ± 9.45
N1 sleep	5.75 ± 4.84
N2 sleep	6.14 ± 3.77
N3 sleep	11.67 ± 8.66

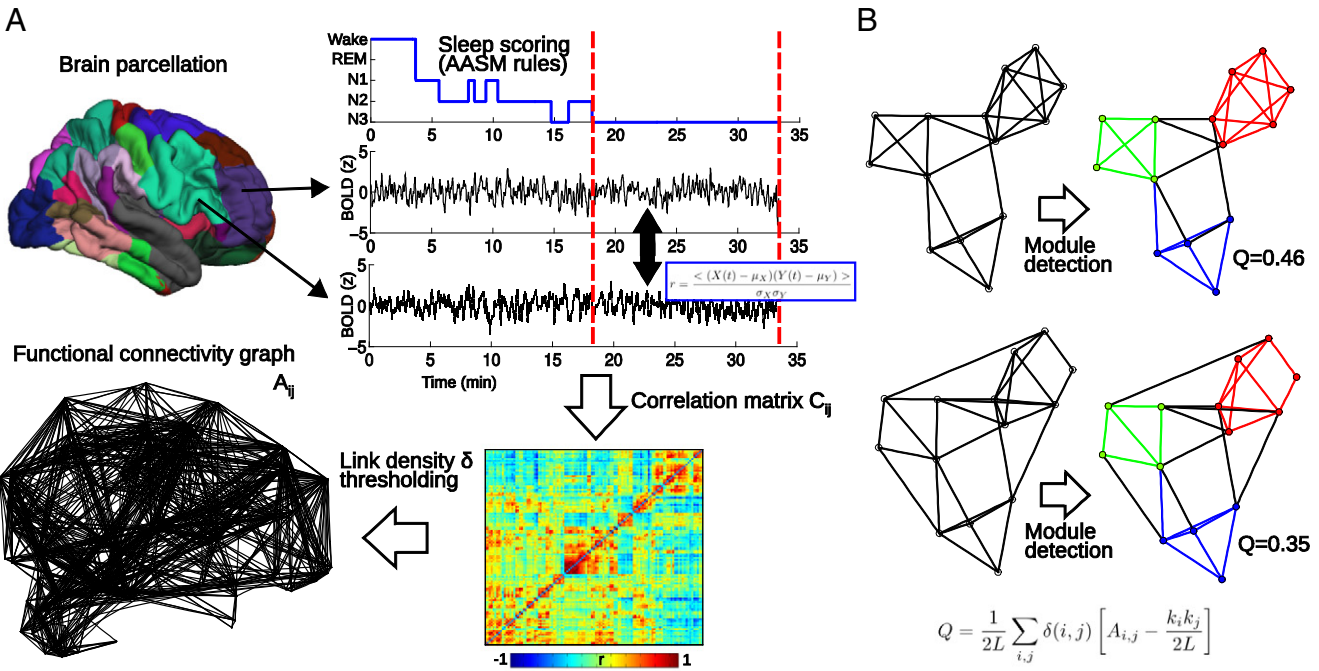


Fig. 1. Schematic description of functional connectivity network construction and examples of modular networks. A) After extraction of average BOLD signals from all regions in the AAL template, the linear correlation coefficient is computed between all region pairs during time periods corresponding to sleep epochs lasting longer than 2 min. The resulting correlation matrix is then thresholded to obtain a functional connectivity graph with link density δ . B) Two examples of module detection using the Louvain algorithm. In the second example, some intra-modular links were randomly rewired as inter-modular connections, resulting in the same modular structure but a lower modularity (Q) value.

each epoch, the Pearson linear correlation coefficient was computed between signals from all pairs of regions as follows,

$$r = \frac{\langle (X(t) - \mu_X)(Y(t) - \mu_Y) \rangle}{\sigma_X \sigma_Y} \quad (1)$$

where $X(t), Y(t)$ are the average BOLD signals from the two regions, $\mu_{X,Y}$ the signal means and $\sigma_{X,Y}$ the standard deviations. This procedure yielded a correlation matrix C_{ij} for each subject and each sleep stage epoch, having on its i,j entry the value of the linear correlation between regions i and j . The final step to obtain functional connectivity graphs was to threshold C_{ij} to yield the binary adjacency matrix A_{ij} which has 1 in its i,j entry if $C_{ij} > \rho$ and 0 otherwise. Values of ρ were selected to adjust networks by link density δ , defined as the ratio between the number of links in the network to the maximum possible number of links. Different correlation thresholds were selected for each network, guaranteeing that all comparisons were made between networks having the same density of links. Otherwise, network properties could be trivially different because of a different total number of links and not due to their re-organization in the network. The relationship between link density and correlation threshold is shown in the Supplementary Information. The δ values considered were in the range $0.025 < \delta < 0.15$ (separated by 0.005 steps). The inferior limit was chosen to avoid dealing with very fragmented networks (Callaway et al., 2000). On the other extreme, very densely connected networks have modularities comparable to those of random networks (approximately $Q \leq 0.3$), making difficult their decomposition into clearly defined functional modules (Reichardt and Bornholdt, 2006).

To construct networks at the group level, i.e. to collapse the information of the single subject adjacency matrices into a single matrix which quantifies interaction strength over the whole population, weighted graphs were introduced (Balenzuela et al., 2010). The corresponding adjacency matrices were obtained by averaging the individual A_{ij} . The resulting weights give an estimate of the reliability of

each individual connection, ranging between 1 (a link between both regions is present in all sleep epochs) and 0 (a link is never found).

Modularity measure and module detection

Heuristically, a module is a subset of nodes in a network which are more densely connected between them than with the rest of the network. A partition of the network is defined as an assignment of all nodes into non-overlapping subsets of nodes. Many mathematical definitions exist to measure the quality of such a partition in terms of module separation, i.e. how well a partition differentiates subsets of nodes tightly connected between them (Fortunato, 2010; Radicchi et al., 2004). A measure of widespread use is that introduced by Newman (Newman and Girvan, 2004). The modularity value assigned to a given partition using this measure is as follows,

$$Q = \frac{1}{2L} \sum_{i,j} \delta(i,j) \left[A_{ij} - \frac{k_i k_j}{2L} \right] \quad (2)$$

where the sum runs over all nodes in the network, L equals the total number of links, $k_i = \sum A_{ij}$ is the degree (number of links attached to node i) and $\delta(i,j) = 1$ if nodes i and j belong to the same subset of the partition, and 0 otherwise. This definition corresponds to an estimate of the difference between the number of intra-modular links and the expected number (for the same partition) in a randomized network of the same size.

The exact determination of the modular structure of a network in terms of modularity maximization requires the evaluation of Q for all possible partitions, a computationally intractable problem (Brandes et al., 2006). This requires the use of algorithms which incorporate a heuristic in the search of the optimal partition. In this paper the Louvain algorithm (Blondel et al., 2008) was applied, as implemented in the Brain Connectivity Toolbox (Rubinov and Sporns, 2010). This algorithm allows computationally efficient module detection through modularity maximization (given by Eq. (2)) and also provides hierarchical information

(the detection of modules within modules). Since the greedy optimization phase of the algorithm is stochastic, throughout the present work the algorithm was applied 1000 times for each network and the partition of higher modularity was kept.

The application of the algorithm to different networks will yield different partitions. In many cases it is important to quantify the similarity between those partitions, for that purpose, we apply the adjusted-for-chance Rand index (Rand, 1971; Steinley, 2004), a measure between 0 (no agreement in the modular structure) and 1 (complete agreement). The adjusted Rand index is comparable to many different measures of clustering similarity (Steinley, 2004).

Time evolving networks and correlation with EEG spectral features

The dynamical evolution of NREM sleep can be correlated with EEG spectral features: light sleep is characterized by a decrease in alpha (8–12 Hz) and an increase in theta (4–8 Hz) band oscillations and deeper stages by a power increase in the slower delta (<4 Hz) band. To study the evolution in time of graph theoretical measures, functional networks must be endowed with dynamical properties. In particular, changes in EEG alpha and delta bands and network modularity during transitions between sleep and wakefulness (termed *arousals*) were studied, as well as the correlation between spontaneous EEG delta power and fMRI functional connectivity fluctuations between regions defined in the AAL template. For these analyses, time evolving functional networks (Bassett et al., 2011) were constructed using a sliding window procedure. The length of the window was set to 2 minutes and for each window the analysis outlined in the previous sections was carried out. This yielded time-dependent correlation $C_{ij}(t)$ and adjacency $A_{ij}(t)$ matrices for which the Louvain algorithm was applied with $\delta=0.075$, resulting in $Q(t)$, the modularity value at each window. Additionally, the EEG power in the aforementioned frequencies was also averaged using a sliding window of the same length.

To study the sharpness of both the modularity and EEG power changes at the onset of a sleep stage transition, the modularity $Q(t)$, alpha and delta power bands (normalized by total EEG power) were extracted from ± 1 minute around the transition (as defined by AASM sleep scoring criteria) and averaged across all transitions and all subjects. This resulted in an average time course for Q and power in alpha and delta bands at sleep to wake transitions (arousals).

$C_{ij}(t)$ contains the dynamical evolution of the functional connectivity between regions i and j . As the vigilance level of the subject fluctuates, changes in the functional network configuration are likewise expected (or vice versa). To analyze whether spontaneous fluctuations in inter-modular functional connectivity over time are related to the vigilance level of the subjects, EEG power in the delta band was used as a vigilance marker and its linear correlation with the (time dependent) functional connectivity values in $C_{ij}(t)$ were computed.

Node roles

Roles can be assigned to nodes depending on their inter and intra-modular connectivity after the identification of the modular structure in the network. In particular, it is of interest to identify those nodes which contribute to the inter-modular connections and those which are very well connected only inside their own modules (Guimerà and Amaral, 2005; Guimerà et al., 2005). A useful measure for this purpose is the z-score of intra-modular degree, defined as

$$z_i = \frac{k_i - \langle k \rangle}{\sigma_k} \quad (3)$$

where k_i represents the intra-modular degree (number of links to the node coming from nodes in the same module), $\langle k \rangle$ and σ_k are the mean and standard deviation of the intra-modular degree, respectively.

The connectivity of the node with nodes in other modules is assessed by the participation coefficient, defined as:

$$P_i = 1 - \sum_j^{N_M} \left(\frac{k_i^{U_j}}{k_i} \right)^2 \quad (4)$$

In this equation N_M is the total number of modules, k_i is the global degree of node i and $k_i^{U_j}$ is the number of links between node i and nodes in module U_j . Using these two indices we divide each node into four categories: provincial hub (high z and low P), connector node (low z and high P), global hub (high z and high P) and provincial node (low z and low P). These categories are defined by selection of arbitrary threshold values z_c and P_c for z and P .

Statistical testing

To test for differences between sleep stages a mixed effects ANOVA was conducted, including a sleep stage factor and subject identification modeled as a random effect to account for possible nested data (different subjects could have different number of sleep epochs of a given sleep stage). Statistical significance of module membership differences was assessed using a permutation testing procedure, as introduced by Alexander-Bloch and colleagues (Alexander-Bloch et al., 2012). Briefly, the within-group similarity (computed with the adjusted-for-chance Rand index) of the real data and permuted data (i.e. randomized data from both groups) was computed. The number of instances in which the within-group similarity of the non-permuted data exceeded that of the permuted data was divided by the number of permutations (in this case, 1000) to obtain the p -value.

Results

Network modularity

In Fig. 2A the modularity (Q) values for all δ are shown (all sleep stages compared to wakefulness). Brain functional networks displayed modular structure with $Q>0.3$ across the whole range of δ values considered. Furthermore, when compared with modularity values from randomized networks (randomized preserving the degree distribution) higher Q was consistently found in the non-randomized networks. Modularity values were significantly higher in N2 and N3 sleep compared to wakefulness for all values of δ , with no significant differences between wakefulness and N1 sleep. No differences in Q were found between N2 and N3 sleep nor between the randomized networks. The average number of modules (N_M) found in the partitions was higher for N1 when compared to wakefulness. No differences were found in N_M for other sleep stages nor for the randomized version of the networks.

Sleep-wake transitions and modularity

To study the dynamical evolution of modularity across vigilance transitions from sleep to wakefulness, time-evolving networks were constructed (at $\delta=0.075$), as described in the methods section. Fig. 3A shows the evolution of modularity averaged across all transitions from deep sleep (N3) to wakefulness (arousals). Fig. 3B shows the same average constructed from EEG power in the delta (1–4 Hz) and alpha (8–12 Hz) bands from a central (C3) and an occipital (O1) channel. These two figures show a strong similarity between the dynamical evolution of EEG and a modularity marker of sleep. Similar network modularity changes were observed for awakenings from N2 sleep, but not during transitions from light to deeper sleep (see Supplementary Information). This similarity was quantified computing the degree of covariance between EEG delta power and modularity values, using the Spearman's rank correlation coefficient (linear correlation between the ranked variables). Scatter plots of fMRI modularity vs. EEG power in

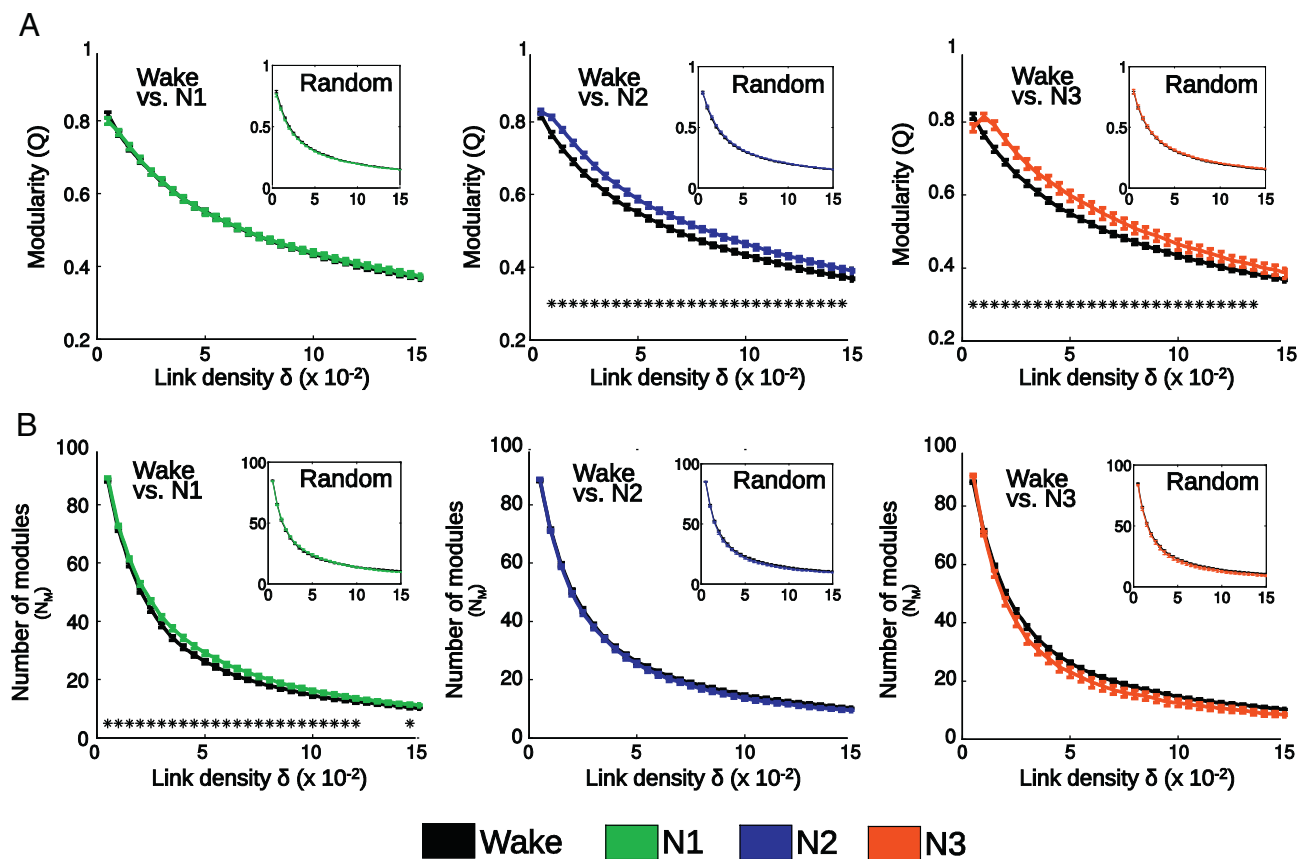


Fig. 2. Network modularity during the descent to deep NREM sleep. A) Mean \pm SEM modularity (Q) is plotted against link density δ for wakefulness together with N1, N2 and N3 sleep respectively. B) Mean \pm SEM number of modules (N_m) as a function of δ for wakefulness together with N1, N2 and N3 sleep respectively (* $p < 0.05$, mixed effects ANOVA). Results for networks after degree-preserving randomization are shown in the insets.

delta and alpha bands are presented in Fig. 3C, together with the Spearman's correlation values ($|\rho| > 0.4$ in all cases). Correlations were highly significant in all cases ($p < 10^{-3}$). In the Supplementary Information we repeat this analysis for EEG power extracted from a frontal channel (F3). We also show how EMG and EOG change time-locked with arousals. Resorting to the subjects who did not fall asleep, we demonstrate that spontaneous hand and leg muscle activation do not induce EEG spectral changes in the delta band nor in network modularity.

Inter-modular functional connectivity changes and power in the EEG delta band

Using a sliding window procedure, an estimate of functional connectivity as a function of time was obtained between the BOLD signals from each pair of regions in the AAL template. The correlation between the dynamical evolution of functional connectivity and power in the EEG delta band was computed for all possible $116 * 115/2$ pairs of regions. Results of this analysis are shown in Fig. 4. No positive correlations survived correction for multiple comparisons. However, widespread negative correlations were found, indicating that increased delta power generally accompanied diminished functional connectivity. Furthermore, inter-modular functional connectivity was more likely to decrease with increasing EEG power in the delta band: only few intra-modular connections in the posterior/occipital module covaried negatively with delta power.

Module membership

Within-group module membership similarity values for actual and permuted data are shown in Fig. 5 for all three comparisons (wakefulness vs. N1, N2 and N3 sleep) and all δ values. Using the

permutation procedure described in the methods section, significant differences in module membership were found in N2 and N3 with respect to wakefulness. No differences were found between N1 and wakefulness, nor between the randomized versions of the networks.

Node roles

The intra-modular degree z score and the participation coefficient P were computed for all networks and modular partitions obtained with the Louvain algorithm. To classify each node in one of the categories described in the methods section, we introduced the thresholds $z_c = 1$ and $P_c = 0.05$. The average number of nodes in each category is plotted for all sleep stages as a function of δ in Fig. 6. N1 sleep was characterized by a decrease in the number of global hubs and an increase in the number of provincial nodes, when compared to wakefulness. The number of provincial hubs was increased both in N2 and N3 (but not in N1) with respect to wakefulness and the number of global hubs was significantly lower in N2. The number of connector nodes was decreased only in N2 at the lower range of δ values.

Node centrality

Results described in the previous section concern differences in the total number of nodes with certain roles in the modular structure, as defined by the z_c and P_c thresholds. To investigate which nodes are involved in these changes, differences in global degree, intra-modular degree z score and participation coefficient (P) were investigated. In Fig. 7 nodes with significant differences in these indexes are shown (Fig. 7A for global degree, Fig. 7B for z and Fig. 7C for P), when wakefulness is compared to N1, N2 and N3 sleep. For N1 sleep a significant decrease of global degree was found in the bilateral thalamus and

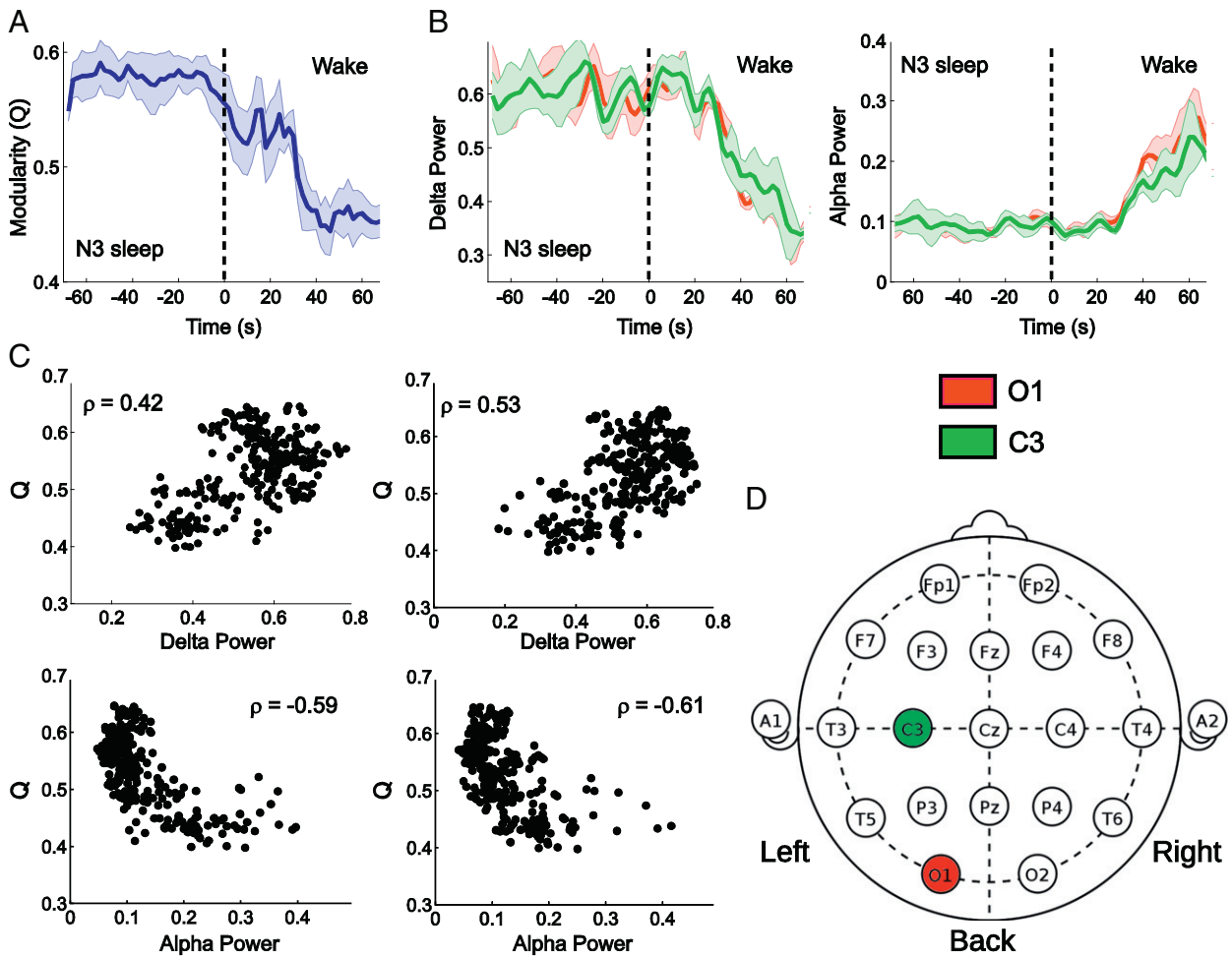


Fig. 3. Network modularity and EEG spectral power in sleep-wake transitions (arousals) A) Modularity (Q) obtained from networks constructed using 2 min sliding windows for linear correlation estimation, averaged across all transitions from N3 sleep to wakefulness. B) Delta (1–4 Hz, left) and alpha (8–12 Hz, right) EEG power temporally averaged with a 2 min sliding window and at all transitions from N3 sleep to wakefulness. C) Scatter plot of EEG delta and alpha power vs. network modularity at all N3-wakefulness transitions, with Spearman rank correlation coefficients (ρ). D) Electrode layout (international 10–20 system).

caudate nucleus. Global degree was increased in nodes corresponding to the calcarine fissure in the primary visual cortex, precuneus and postcentral gyrus. No differences were found for intra-modular degree z score and P . For N2 sleep, a decrease in global degree was found in the bilateral lingual and fusiform gyri, middle and inferior temporal gyri, and inferior occipital gyri, with an increase in motor areas including SMA and paracentral lobule, precuneus, middle and posterior cingulate gyri and primary auditory cortex (Heschl's gyrus). Patterns of changes in P and z were similar for N2, comprising a decrease in the fusiform gyrus and an increase in the bilateral poles of the temporal lobes, Heschl's gyrus and calcarine fissure. During N3 sleep the global degree decreased in superior temporal and fusiform gyri and increased in the posterior cingulate cortex. Both z and P were decreased in the bilateral superior temporal gyri.

Group averaged networks and module membership in weighted networks

The previous analyses yielded one value of the optimal modularity for each sleep stage and each subject as well as an optimal partition into functional modules. To obtain a partition at the group level, individual adjacency matrices were averaged and the weighted version of the Louvain algorithm was applied. The resulting Q values and N_M are shown in Fig. 8A. As obtained for the individual networks, Q increased from wakefulness to deep (N3) sleep. The modularity values for the group averaged networks showed a gradual increase, with N2 having smaller values than N3. The number of modules associated with these modularity values had

a plateau of $N_M=5$ for $\delta>0.05$. Similarity of the module memberships with respect to a reference partition at $\delta=0.075$ (Fig. 8B, left) demonstrated agreement with $RI>0.80$, suggesting a relatively stable modular structure over this range. Similarity values of module membership between N1, N2 and N3 sleep with respect to wakefulness are shown in Fig. 8B (right) as a function of δ . The adjusted-for-chance Rand index progressively decreased as sleep depth increased, reaching a minimum of $RI\approx 0.4$ for N3 sleep. Results of node roles in the modular structure of group averaged networks are shown in Fig. 8C. The number of provincial nodes and provincial hubs increased from wakefulness to deep sleep, while the number of hubs decreased (having a maximum during N1 sleep), as well as the number of connector nodes.

The application of the Louvain algorithm to the group averaged networks allowed to determine the distribution of nodes into modules. Results are shown in Figs. 9A and B for module membership at $\delta=0.075$. A total of 5 modules were found at this δ value. Modules can be summarized as follows:

Central module: comprised primary motor and somatosensory cortices, supplementary motor area, language areas in the supramarginal gyrus and the bilateral insular cortices. As sleep deepened this module engaged areas from the fronto/parietal module (dorsal and anterior cingulate cortex). N1 sleep was marked by a further engagement of regions from the frontal/parietal module (inferior frontal gyrus and the orbital part of the inferior frontal gyrus).

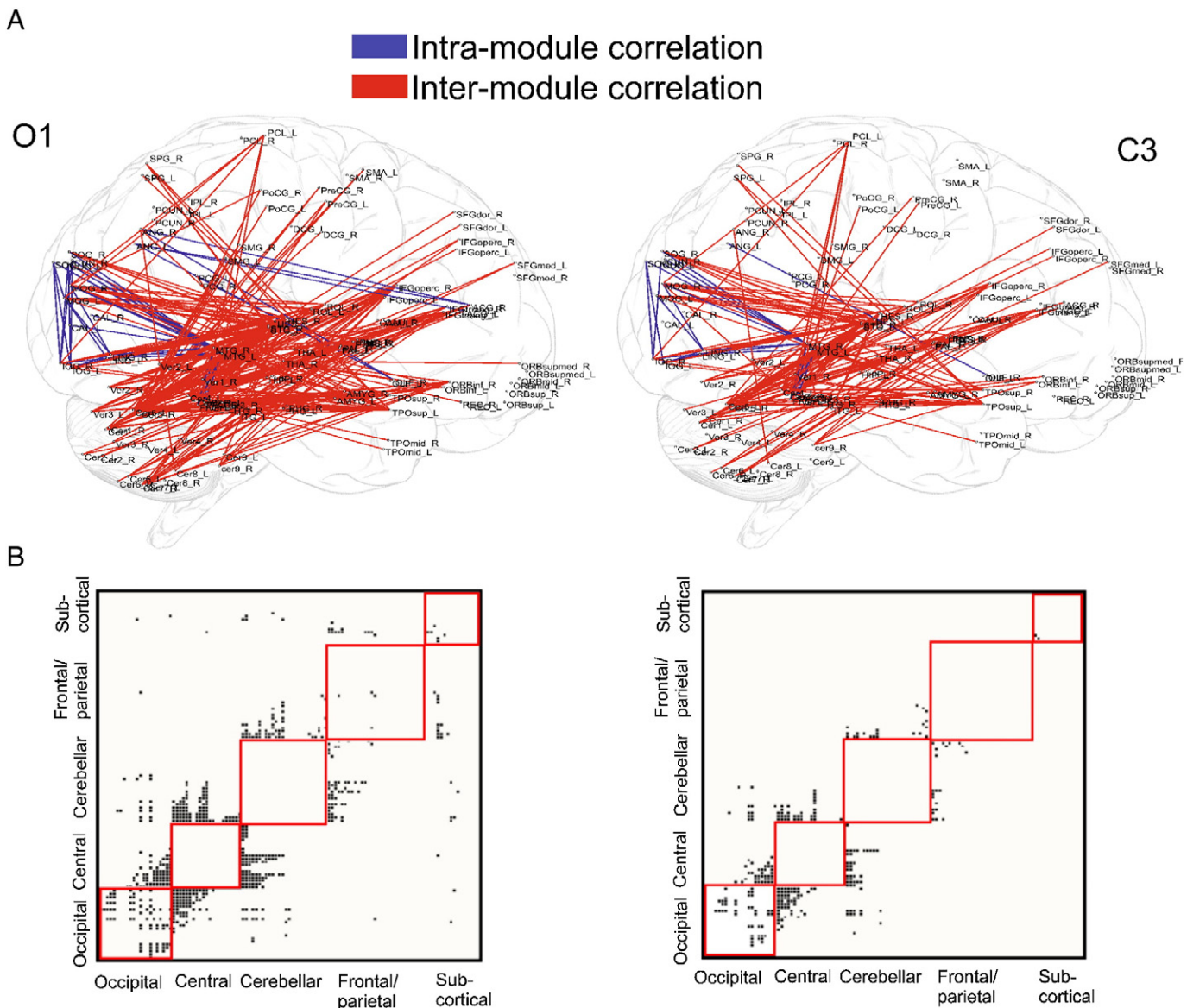


Fig. 4. Anatomical overlay of links representing negative correlations between functional connectivity fluctuations of the connected regions and spontaneous fluctuations of EEG delta power (A) and the same results presented in adjacency matrix form (B). Links, or non-empty (black) matrix entries, represent significant negative correlations with $p < 0.05$, Bonferroni corrected for multiple comparisons ($n = 116 \times 115/2$). Results are shown for occipital (O1) and central (C3) EEG delta power.

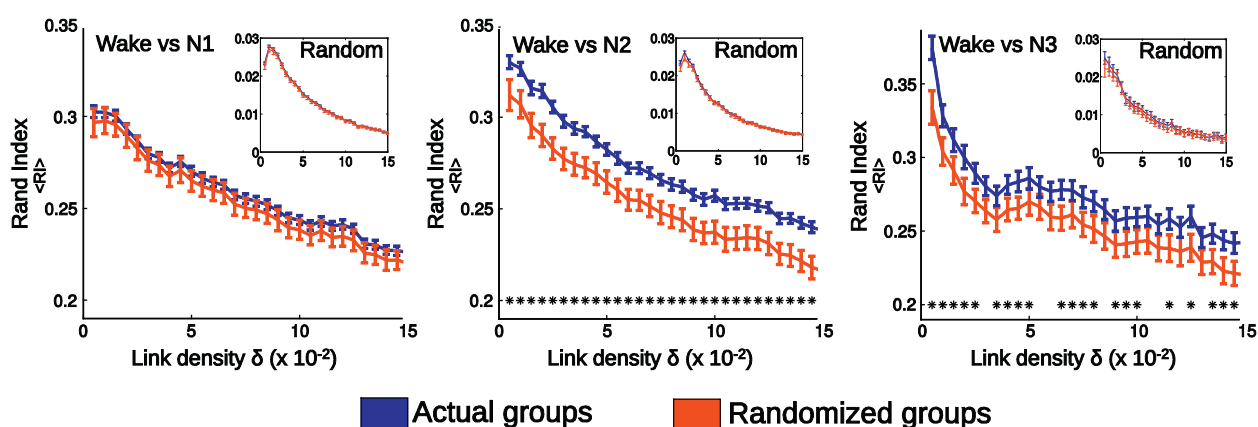


Fig. 5. Mean \pm SD within-group similarity (measured with RI) of modular partitions as a function of link density δ for actual data and randomized group labels (* $p < 0.05$, p -value obtained using a permutation test with 1000 permutations). Results for networks after degree-preserving randomization are shown in the insets.

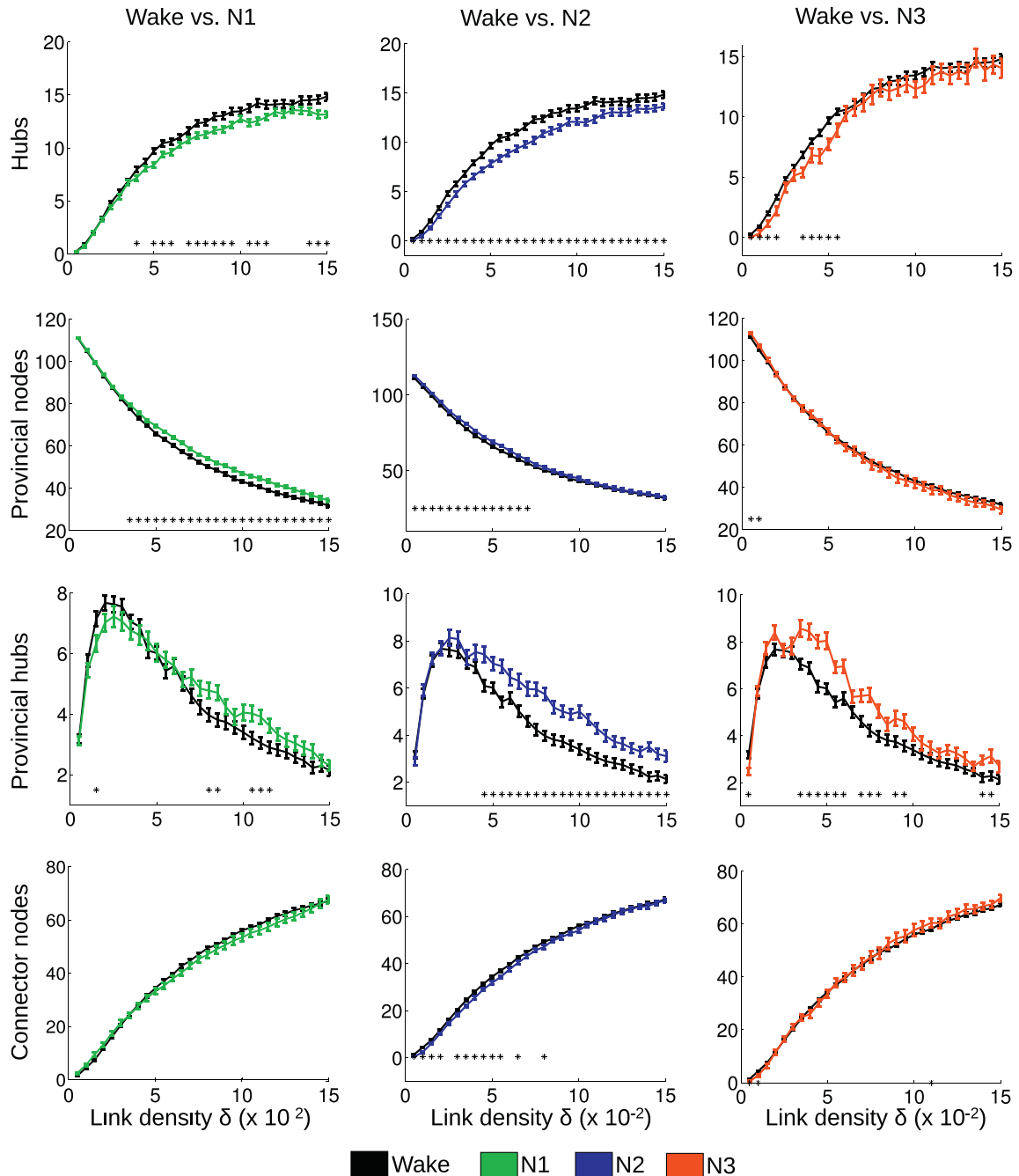


Fig. 6. Mean \pm SEM number of nodes in each category, defined by $z_c = 1$ and $P = 0.05$ (global hubs, provincial nodes, provincial hubs and connector nodes), as a function of link density δ for wakefulness together with N1, N2 and N3 sleep ($^*p < 0.05$, mixed effects ANOVA).

Cerebellar module: comprised all cerebellar regions. During N3 sleep the thalamus was dissociated from the subcortical module and engaged in the cerebellar module.

Frontal/parietal module: comprised frontal and parietal regions. The spatial distribution of these regions roughly resembled those involved in the DMN. As sleep deepened, this module lost cingulate and frontal regions to the central module. In N2 and N3 sleep it consisted solely of parietal and frontal regions and fragments of the inferior temporal lobes.

Subcortical: this module consisted of subcortical regions as well as the hippocampus and para-hippocampus. It was stable during all sleep stages, except in N3 sleep, when the thalamus disengaged.

Posterior/occipital module: comprised primary and secondary visual cortices as well as areas of the visual stream in the inferior temporal gyrus, both during wakefulness and N1 sleep. As sleep deepened, these higher order visual areas disengaged from the network and engaged in the frontal/parietal module.

Discussion

We analyzed brain modular structure during the gradual loss of vigilance which accompanies the descent to deep sleep and observed an increase in functional segregation with the onset of N2 and further with N3 sleep, which quickly decreased after arousals (awakenings from deep sleep). N1 sleep, on the other hand, had a very similar

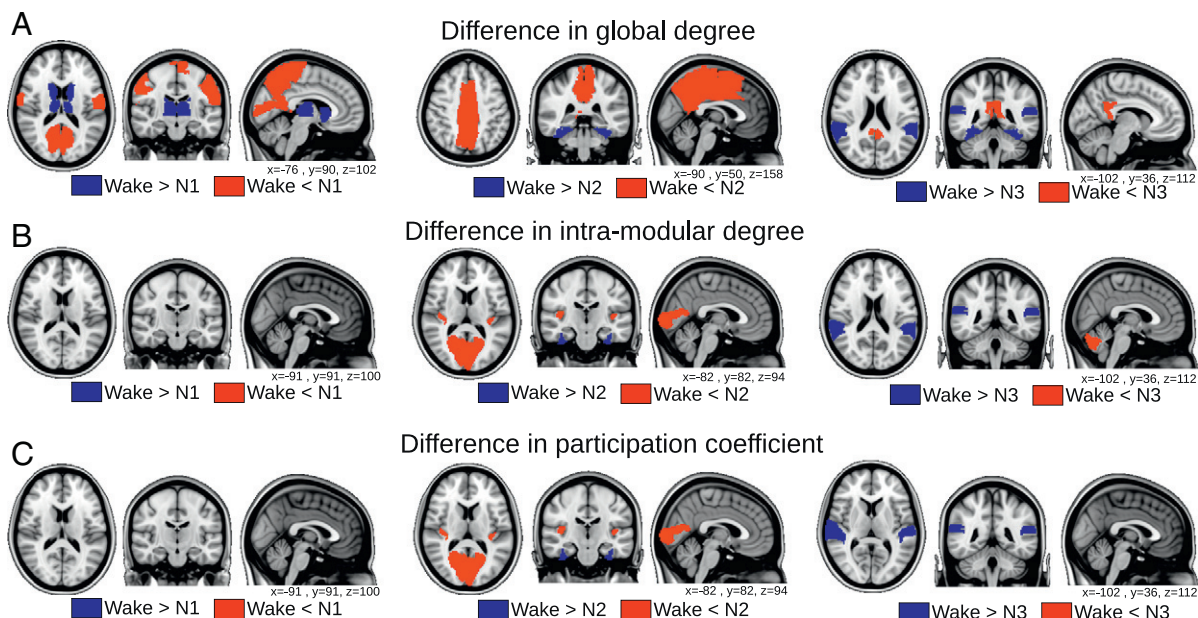


Fig. 7. AAL regions with statistically significant differences in global degree (A), intra-modular degree z-score (B) and participation coefficient (C) (mixed effects ANOVA, Bonferroni corrected for multiple comparisons, $n = 116$).

structure compared to wakefulness, both in terms of segregation and functional module membership. EEG delta power changes paralleled functional segregation between modules, with loss of functional connectivity between them occurring at times of high delta power. In deeper sleep stages, nodes were re-organized between modules as well as with respect to their roles in the modular structure: the number of locally well-connected hubs was increased and the number of globally well-connected hubs decreased.

Network modularity changes and conscious content during NREM sleep

A recent study (Boly et al., 2012) demonstrated increased functional segregation between wakefulness and all stages of NREM sleep combined together. These changes were interpreted as reflecting reduced conscious content during sleep compared to wakefulness. However, NREM sleep is not homogeneous regarding awareness, responsiveness and conscious content. The sub-division of NREM sleep based on EEG features (AASM, 2007) closely parallels behavioral and cognitive changes. Awakenings from light (N1) sleep are usually characterized by recollections of vivid hypnagogic hallucinations and lucid dreams (Domhoff, 2002; Kusse et al., 2011), as well as by cognitive manipulations sharing similarities with those performed during wakefulness (Stickgold et al., 2000; Wamsley et al., 2010). The production of conscious content in the form of hypnagogic hallucinations has been related to thalamic deactivation during early sleep, which can temporally precede changes in cortical activity by several minutes (Magnin et al., 2010). In this situation, the cortex can display patterns of activity resembling wakefulness in spite of thalamic disconnection. Behaviorally, subjects during N1 sleep are even capable of simple tasks (Casagrande et al., 1997; Ogilvie and Wilkinson, 1984). Early sleep is characterized by different response patterns elicited by sensory stimulation (Campbell and Colrain, 2002; Czisch et al., 2004), when compared to those obtained during deeper sleep stages (Schabus et al., 2012). During these stages (starting from N2 sleep) sensory awareness starts vanishing and dream reports after awakenings become less vivid than those obtained during light and REM sleep (McNamara et al., 2010). Our large body of data allowed us to directly test for network modularity changes specific to each sleep stage. In light of these studies, if functional integration indeed parallels conscious content (as hypothesized by Boly and colleagues (2012)) changes in network modularity are expected for deep (N2 and N3) sleep compared to

N1 sleep and wakefulness. Increased functional segregation was indeed found only during N2 and N3 sleep, in contrast, integration was preserved during light (N1) sleep. Since we did not probe the conscious experience directly (for example, obtaining a report for each awakening) our suggestion that network modularity parallels the degree of conscious content remains an indirect one. However, changes in functional segregation observed across different vigilance states previously associated with variable levels of conscious content appear to suggest such a relationship.

From a mathematical point of view, network modularity is suggestive of previously introduced measures of information integration (Tononi, 2005; Tononi and Edelman, 1998). Modularity represents the optimal value of a cost function measuring how well nodes are separated into interacting (integrated) but distinct (segregated) functional modules. Thus, the optimal modular structure cannot be decomposed into smaller subsets without a decrease in modularity values. This property is shared by the minimum information partition (Tononi, 2004), which is used to define the amount of integrated information generated by the system, and hence is an obvious starting point to analytical hypothesis testing about the relationship between information-theoretical measures of consciousness and large-scale functional brain network architecture. Finally, loss of inter-modular connectivity during deep sleep is consistent with the breakdown of long-range effective connectivity observed during slow wave sleep after a localized perturbation is induced (Massimini et al., 2005).

Correlation with EEG spectral power

While correlations between fMRI observables and EEG vigilance markers have been previously reported (Boly et al., 2012; Horovitz et al., 2008), the dynamical evolution of fMRI-based vigilance measures during sleep stage transitions remained an interesting open issue. Our results show that awakenings from deep sleep cause a sharp decrease in network modularity. This decrease occurs at a time-scale comparable to the observed changes in EEG spectral power and can be rooted in the need to quickly revert to a fully conscious state in the presence of an environmental demand. It is important to remark that sleep staging of 30 s EEG epochs (AASM, 2007) imposes a temporal resolution limit, thus finer sleep staging methods could reveal an even sharper transition in EEG spectral power predicting changes in

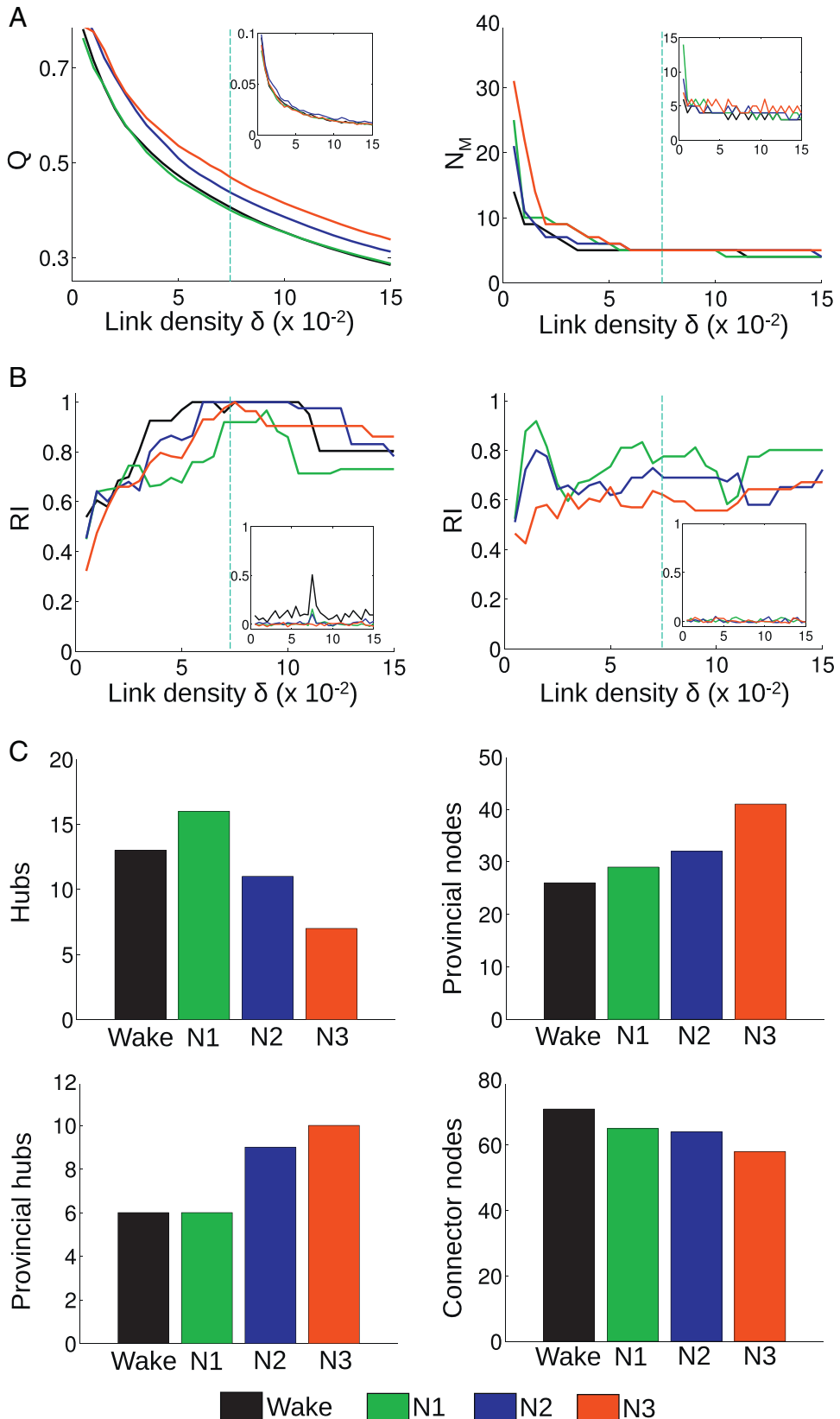


Fig. 8. Results for modularity analysis of group averaged functional connectivity networks. A) Left: modularity (Q) for wakefulness, N1, N2 and N3 sleep as function of link density δ . Right: Number of modules (N_M) as a function of δ . B) Left: Rand index with a reference partition at $\delta = 0.075$ as a function of δ for all sleep stages. Right: Rand index between the modular partition at wakefulness and the N1, N2 and N3 modular partitions, as a function of δ . In all cases, the equivalent results for networks after degree-preserving randomization are shown in the insets C) Number of nodes in each category for all sleep stages.

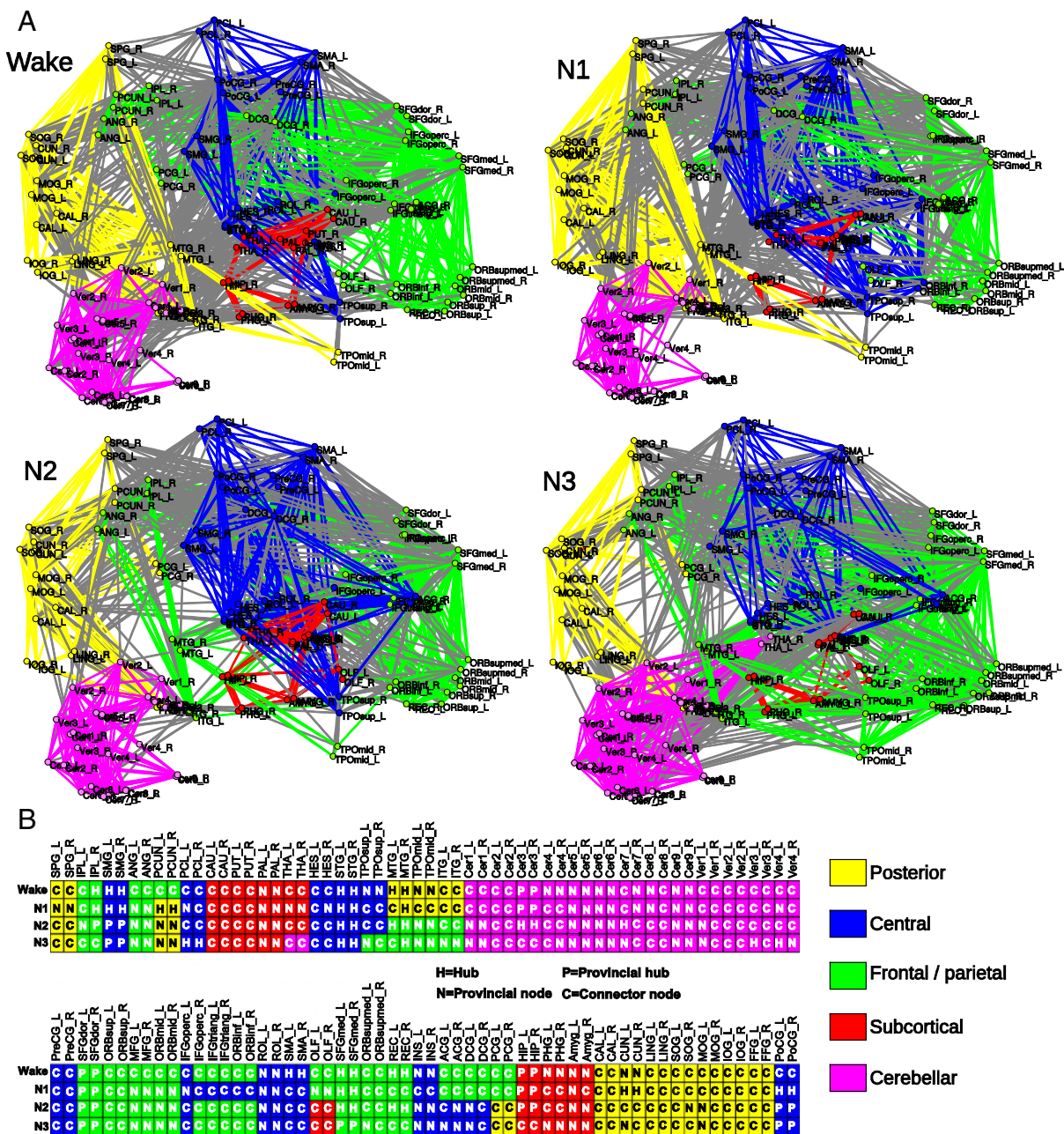


Fig. 9. The modular structure of group averaged connectivity networks at $\delta = 0.075$. A) Graph representation of the networks in anatomical space (each node is located at the center of mass of the corresponding AAL region). Inter-modular links are colored in gray, intra-modular links are color coded for each one of the five modules. B) Information on module membership and node role for each one of the 116 regions in the AAL template.

fMRI network modularity (or vice-versa). The computation of time-locked averages in the transition from N1 to N2 sleep (two sleep stages associated with different modularity values) did not reveal sharp changes like those observed during awakenings. We must note, however, that the process of falling asleep appears to be more gradual in terms of EEG spectral content changes (De Gennaro et al., 2001). Furthermore, brain activity alterations in the descent to sleep appear asynchronously in cortical and sub-cortical structures, but are quickly and synchronously reverted during awakenings (Magnin et al., 2010).

Another relevant result concerns the negative correlation between EEG delta power and spontaneous functional connectivity fluctuations in inter-modular links. Non-stationarities in the dynamical coordination (measured with BOLD fMRI) between brain regions have been recently described by different methods (Chang and Glover,

2010; Hutchison et al., 2012). The physiological causes underlying those fluctuations remain a subject of study. It can be speculated that ongoing spontaneous cognitive operations modulate the dynamics of large-scale network coordination during the resting state. Nevertheless, our finding reveals that a certain subset of those fluctuations (corresponding to inter-modular connectivity) can be explained in terms of vigilance fluctuations, given the negative correlation with classical EEG markers of vigilance. Thus, EEG delta power and functional segregation are remarkably interrelated: an EEG practitioner has indirect access to these large-scale functional measures simply by looking at scalp delta power. This observation might be interestingly extended from sleep to generalized and focal slowing such as in encephalopathy, localized brain damage or also during epileptic seizures, topics deserving further investigation.

Re-arrangement of modular structure during sleep

It could be possible that only changes in functional integration/segregation characterize different stages of NREM sleep, without any re-arrangement of brain regions in the functional modules. So far this question has only been addressed at the level of RSN and with conflicting results. Surprisingly, most RSN are stable during light sleep and deeper sleep stages (Boly et al., 2008, 2012; Larson-Prior et al., 2009), the sole exception being the DMN, in which posterior-anterior disconnection patterns were observed (Horovitz et al., 2009; Sämann et al., 2011). Here, we addressed the question of functional module membership specifically for each stage of NREM sleep using recently introduced permutation methods (Alexander-Bloch et al., 2012). We found that modules are re-organized only during N2 and N3 sleep. N1 organization, on other hand, remained similar to wakefulness. The precise nature of these changes was further explored by group averaged networks (see discussion on **Module membership** below), pointing to alterations in the frontal/parietal module, which comprises many key DMN regions.

Node roles in the modular structure

The observed decrease in the number of hubs during N1, induced by the disconnection of the thalamus from cortical nodes, has been previously discussed as a factor leading to topological changes such as alterations in the small-world properties of the functional networks (Spoormaker et al., 2010). However, localized connectivity decreases are not necessarily followed by a modularity increase: we showed, for example, that thalamic links lost during N1 sleep did not re-arrange to strengthen intra-modular connectivity and therefore segregation did not increase in early sleep. In contrast, N2 sleep was marked not only by a decrease in the number of nodes cataloged as global hubs but also by an increment in the number of provincial hubs, a trend preserved during N3 sleep. These nodes accumulated intra-modular connections and contributed to increased modularity values. Analysis of the nodes involved with these changes revealed many sensory areas. While sensory effective disengagement is a prerequisite for sleep, our results point to the intriguing possibility that disengagement of these areas has an active effect in facilitating the integration breakdown.

Module membership

Five functional modules were found, which showed substantial re-configuration in the progression to deep sleep. The largest membership changes observed concerned a disengagement of higher order visual areas from the posterior/occipital module in N2/N3 sleep and a rearrangement of the whole cingulate cortex from the frontal/parietal to the central module. Loss of visual imagery can account for the disintegration of the posterior module, which coordinates lower and higher order visual areas during wakefulness and early sleep. Interestingly, nodes corresponding to regions active in other sensory modalities (e.g. auditory) did not change module membership, a possible consequence of the processing of ongoing environmental stimuli. This observation is consistent with similarly preserved sensory connectivity under Propofol anesthesia (Boveroux et al., 2010). The disengagement of anterior cingulate regions from frontal-parietal regions can be related to decreased connectivity between regions in the ventromedial prefrontal cortex (VMPFC), involved in higher executive functions such as decision making or social cognition (Muzur et al., 2002), which are not executed during sleep. The onset of slow wave sleep has been shown to deactivate anterior cingulate regions (Maquet et al., 1997), which could also hinder their interaction with other constituents of the VMPFC. Posterior cingulate structures play a pivotal role in the maintenance of the DMN during wakefulness (Fransson and Marrelec, 2008). The breakdown of the frontal-parietal module is likely related to the disintegration of the

DMN, previously observed by different methods (Horovitz et al., 2009; Sämann et al., 2011). Finally, insights from other states of impaired consciousness, such as epilepsy, point to abnormal deactivations in default mode regions (Gotman et al., 2005; Kobayashi et al., 2006; Laufs et al., 2007b).

Conclusions

In conclusion, our results demonstrate that network modularity increases with the loss of conscious awareness characteristic of deep sleep, signaling a breakdown of the integration between functional modules. EEG delta power closely parallels these large-scale network changes, both during arousals from sleep to wakefulness and also in its spontaneous fluctuations, which negatively correlate with inter-modular connectivity fluctuations as measured with fMRI. Furthermore, module membership is re-shaped during the descent to deep sleep and, together with the determination of node roles in the modular structure, sheds light on the mechanisms underlying the collapse of inter-modular interactions. Further exploration of the relationship between measures of functional network modularity and neural complexity should be undertaken to establish a closer link between information integration theories of consciousness and our results.

Acknowledgments

This work was funded by the Bundesministerium für Bildung und Forschung (grant 01 EV 0703) and the LOEWE Neuronale Koordination Forschungsschwerpunkt Frankfurt (NeFF). The authors declare no competing financial interests. We thank Torben E. Lund for providing a MATLAB implementation of the RETROICOR method, Sandra Anti, Ralf Deichmann and Steffen Volz for extensive MRI support and all subjects for their participation.

Appendix A. Supplementary data

Supplementary data to this article can be found online at <http://dx.doi.org/10.1016/j.neuroimage.2012.12.073>.

References

- AASM, 2007. The AASM manual for the scoring of sleep and associated events-rules. Terminology and technical specifications. American Academy of Sleep Medicine, Chicago.
- Achard, S., Bullmore, E., 2007. Efficiency and cost of economical brain functional networks. *PLoS Comput. Biol.* 3, e17. <http://dx.doi.org/10.1371/journal.pcbi.0030017>.
- Achard, S., Salvador, R., Whitcher, B., Suckling, J., Bullmore, E., 2006. A resilient, low-frequency, small-world human brain functional network with highly connected association cortical hubs. *J. Neurosci.* 26, 63–72.
- Alexander-Bloch, A.F., Gogtay, N., Meunier, D., Birn, R., Clasen, L., Lalonde, F., Lenroot, R., Giedd, J., Bullmore, E.T., 2010. Disrupted modularity and local connectivity of brain functional networks in childhood-onset schizophrenia. *Front. Syst. Neurosci.* 4, 147.
- Alexander-Bloch, A., Lambiotte, R., Roberts, B., Giedd, J., Gogtay, N., Bullmore, E., 2012. The discovery of population differences in network community structure: new methods and applications to brain functional networks in schizophrenia. *NeuroImage* 59, 3889–3900.
- Allen, P.J., Polizzi, G., Krakow, K., Fish, D.R., Lemieux, L., 1998. Identification of EEG events in the MR scanner: the problem of pulse artifact and a method for its subtraction. *NeuroImage* 8, 229–239.
- Balenzuela, P., Chernomoretz, A., Fraiman, D., Cifre, I., Sitges, C., Montoya, P., Chialvo, D.R., 2010. Modular organization of brain resting state networks in chronic back pain patients. *Front. Neuroinform.* 4, 116.
- Bassett, D.S., Bullmore, E., 2006. Small-world brain networks. *Neuroscientist* 12, 512–523.
- Bassett, D.S., Bullmore, E., Verchinski, B.A., Mattay, V.S., Weinberger, D.R., Meyer-Lindenberg, A., 2008. Hierarchical organization of human cortical networks in health and schizophrenia. *J. Neurosci.* 28, 9239–9248.
- Bassett, D.S., Wymbs, N.F., Porter, M.A., Mucha, P.J., Carlson, J.M., Grafton, S.T., 2011. Dynamic reconfiguration of human brain networks during learning. *Proc. Natl. Acad. Sci.* 108, 7641–7646.
- Beckmann, C., DeLuca, M., Devlin, J.T., Smith, S.M., 2005. Investigations into resting-state connectivity using independent component analysis. *Phil. Trans. R. Soc. B* 360, 1001–1013.

- Blondel, V.D., Guillaume, J.L., Lambiotte, R., Lefebvre, E., 2008. Fast unfolding of communities in large networks. *J. Stat. Mech.* P10008.
- Boly, M., Phillips, C., Tshibanda, L., Vanhaudenhuyse, A., Schabus, M., Dang-Vu, T.T., Moonen, G., Hustinx, R., Maquet, P., Laureys, S., 2008. Intrinsic brain activity in altered states of consciousness. *Ann. N. Y. Acad. Sci.* 1129, 119–129.
- Boly, M., Perlberg, V., Marrelec, G., Schabus, M., Laureys, S., Doyon, J., Péligrini-Issac, M., Maquet, P., Benali, H., 2012. Hierarchical clustering of brain activity during human non-rapid eye movement sleep. *Proc. Natl. Acad. Sci.* 109, 5856–5861.
- Boveroux, P., Vanhaudenhuyse, A., Bruno, M.A., Noirhomme, Q., Lauwick, S., Luxen, A., Degueldre, C., Plenevaux, A., Schnakers, C., Phillips, C., Brichant, J.F., Bonhomme, V., Maquet, P., Greicius, M., Laureys, S., Boly, M., 2010. Breakdown of within- and between-network Resting State Functional Magnetic Resonance Imaging connectivity during propofol-induced loss of consciousness. *Anesthesiology* 113, 1038–1053.
- Brandes, U., Delling, D., Gaertler, M., Goerke, R., Hoefer, M., Nikoloski, Z., Wagner, D., 2006. Maximizing modularity is hard (arXiv Physics 0608255).
- Britz, J., van De Ville, D., Michel, C.M., 2010. BOLD correlates of EEG topography reveal rapid resting-state network dynamics. *Neuroimage* 52, 1162–1170.
- Brodebeck, V., Kuhn, A., von Wegner, F., Morzelewski, A., Tagliazucchi, E., Borisov, S., Michel, C.M., Laufs, H., 2012. EEG microstates of wakefulness and NREM sleep. *Neuroimage* 62, 2129–2139.
- Bullmore, E.T., Sporns, O., 2009. Complex brain networks: graph theoretical analysis of structural and functional systems. *Nat. Rev. Neurosci.* 10, 186–198.
- Callaway, D.S., Newman, M.E.J., Strogatz, S.H., Watts, D.J., 2000. Network robustness and fragility: percolation on random graphs. *Phys. Rev. Lett.* 85, 5468–5471.
- Campbell, K.B., Colrain, I.M., 2002. Event-related potential measures of the inhibition of information processing: II. The sleep onset period. *Int. J. Psychophysiol.* 46, 197–214.
- Casagrande, M., De Gennaro, L., Violani, C., Braibanti, P., Bertini, M., 1997. A finger-tapping task and a reaction time task as behavioral measures of the transition from wakefulness to sleep: which task interferes less with the sleep onset process. *Sleep* 20, 301–312.
- Chang, C., Glover, G.H., 2010. Time-frequency dynamics of resting-state brain connectivity measured with fMRI. *Neuroimage* 50, 81–98.
- Cordes, D., Haughton, V.M., Arfanakis, K., Carew, J.D., Turski, P.A., Moritz, C.H., Quigley, M.A., Meyerand, M.E., 2001. Frequencies contributing to functional connectivity in the cerebral cortex in "resting-state" data. *Am. J. Neuroradiol.* 22, 1326–1333.
- Czisch, M., Wehrle, R., Kauffmann, C., Wetter, T.C., Holsboer, F., Pollmächer, T., Auer, D.P., 2004. Functional MRI during sleep: BOLD signal decreases and their electrophysiological correlates. *Eur. J. Neurosci.* 20, 566–574.
- De Gennaro, L., Ferrara, M., Bertini, M., 2001. The boundary between wakefulness and sleep: quantitative electroencephalographic changes during the sleep onset period. *Neuroscience* 107, 1–11.
- de Haan, W., van der Flier, W.M., Koene, T., Smits, L.L., Scheltens, P., Stam, C.J., 2012. Disrupted modular brain dynamics reflect cognitive dysfunction in Alzheimer's disease. *Neuroimage* 59, 3085–3093.
- Dornhoff, G.W., 2002. The Scientific Study of Dreams. American Psychological Association, Washington, D.C.
- Eguíluz, V.M., Chialvo, D.R., Cecchi, G.A., Baliki, M., Apkarian, A.V., 2005. Scale-free brain functional networks. *Phys. Rev. Lett.* 94, 018102.
- Fortunato, S., 2010. Community detection in graphs. *Phys. Rep.* 486, 75–174.
- Fransson, P., Marrelec, G., 2008. The precuneus/posterior cingulate cortex plays a pivotal role in the default mode network: evidence from a partial correlation network analysis. *Neuroimage* 42, 1178–1184.
- Glover, G.H., Li, T.Q., Ress, D., 2000. Image-based method for retrospective correction of physiological motion effects in fMRI: RETROICOR. *Magn. Reson. Med.* 44, 162–167.
- Gotman, J., Grova, C., Bagshaw, A., Kobayashi, E., Aghakhani, Y., Dubeau, F., 2005. Generalized epileptic discharges show thalamocortical activation and suspension of the default state of the brain. *Proc. Natl. Acad. Sci.* 102, 15236–15240.
- Guimerà, R., Amaral, L.A.N., 2005. Functional cartography of complex metabolic networks. *Nature* 433, 895–900.
- Guimerà, R., Mossa, S., Turtschi, A., Amaral, L.A.N., 2005. The worldwide air transportation network: anomalous centrality, community structure, and cities global roles. *Proc. Natl. Acad. Sci.* 102, 7794–7799.
- Horowitz, S.G., Fukunaga, M., de Zwart, J.A., van Gelderen, P., Fulton, S.C., Balkin, T.J., Duyn, J.H., 2008. Low frequency BOLD fluctuations during resting wakefulness and light sleep: a simultaneous EEG-fMRI study. *Hum. Brain Mapp.* 29, 671–682.
- Horowitz, S.G., Braun, A.R., Carr, W.S., Picchioni, D., Balkin, T.J., Fukunaga, M., Duyn, J.H., 2009. Decoupling of the brain's default mode network during deep sleep. *Proc. Natl. Acad. Sci.* 106, 11376–11381.
- Hutchison, R.M., Womelsdorf, T., Gati, J.S., Everling, S., Menon, R.S., 2012. Resting-state networks show dynamic functional connectivity in awake humans and anesthetized macaques. *Hum. Brain Mapp.* <http://dx.doi.org/10.1002/hbm.22058>.
- Jahnke, K., von Wegner, F., Morzelewski, A., Borisov, S., Maischein, M., Steinmetz, H., Laufs, H., 2011. To wake or not to wake? The two-sided nature of the human K-complex. *Neuroimage* 59, 1631–1638.
- Kobayashi, E., Bagshaw, A.P., Grova, C., Dubeau, F., Gotman, J., 2006. Negative BOLD responses to epileptic spikes. *Hum. Brain Mapp.* 27, 488–497.
- Kusse, C., Shaffii-Le, B.A., Schrouff, J., Matarazzo, L., Maquet, P., 2011. Experience-dependent induction of hypnagogic images during daytime naps: a combined behavioural and EEG study. *J. Sleep Res.* 21, 10–20.
- Larson-Prior, L.J., Zempel, J.M., Nolan, T.S., Prior, F.W., Snyder, A.Z., Raichle, M.E., 2009. Cortical network functional connectivity in the descent to sleep. *Proc. Natl. Acad. Sci.* 106, 4489–4494.
- Laufs, H., Walker, M.C., Lund, T.E., 2007a. Brain activation and hypothalamic functional connectivity during human non-rapid eye movement sleep: an EEG/fMRI study (author reply). *Brain* 130, e75.
- Laufs, H., Hamandi, K., Salek-Haddad, A., Kleinschmidt, A.K., Duncan, J.S., Lemieux, L., 2007b. Temporal lobe interictal epileptic discharges affect cerebral activity in "default mode" brain regions. *Hum. Brain Mapp.* 28, 1023–1032.
- Magnin, M., Rey, M., Bastuji, H., Guillemant, P., Mauguiere, F., Garcia-Larrea, L., 2010. Thalamic deactivation at sleep onset precedes that of the cerebral cortex in humans. *Proc. Natl. Acad. Sci. U. S. A.* 107, 3829–3833.
- Maquet, P., Degueldre, C., Delfiore, G., Aerts, J., Péters, J.M., Luxen, A., Franck, G., 1997. Functional neuroanatomy of human slow wave sleep. *J. Neurosci.* 17, 2807–2812.
- McNamara, P., Johnson, P., McLaren, D., Harris, E., Beauharnais, C., Auerbach, S., 2010. REM and NREM sleep mentation. *Int. Rev. Neurobiol.* 92, 69–86.
- Meunier, D., Lambiotte, R., Fornito, A., Ersche, K.D., Bullmore, E.T., 2009a. Hierarchical modularity in human brain functional networks. *Front. Neuroinform.* 3, 37.
- Meunier, D., Achard, S., Morcom, A., Bullmore, E., 2009b. Age-related changes in modular organization of human brain functional networks. *Neuroimage* 44, 715–723.
- Muzur, A., Pace-Schott, E.F., Hobson, J.A., 2002. The prefrontal cortex in sleep. *Trends Cogn. Sci.* 6, 475–481.
- Newman, M.E.J., Girvan, M., 2004. Finding and evaluating community structure in networks. *Phys. Rev. E* 69, 026113.
- Ogilvie, R.D., Wilkinson, R.T., 1984. The detection of sleep onset: behavioral and physiological convergence. *Psychophysiology* 21, 510–520.
- Radicchi, F., Castellano, C., Cecconi, F., Loreto, V., Parisi, D., 2004. Defining and identifying communities in networks. *Proc. Natl. Acad. Sci.* 101, 2658–2663.
- Raichle, M.E., MacLeod, A.M., Snyder, A.Z., Powers, W.J., Gusnard, D.A., Shulman, G.L., 2001. A default mode of brain function. *Proc. Natl. Acad. Sci.* 98, 676–682.
- Rand, W.M., 1971. Objective criteria for the evaluation of clustering methods. *J. Am. Stat. Assoc.* 66, 846–850.
- Reichardt, J., Bornholdt, S., 2006. When are networks truly modular? *Physica D* 224, 20–26.
- Rubinov, M., Sporns, O., 2010. Complex network measures of brain connectivity: uses and interpretations. *Neuroimage* 52, 1059–1069.
- Sämann, P.G., Wehrle, R., Hoehn, D., Spoormaker, V.I., Peters, H., Tully, C., Holsboer, F., Czisch, M., 2011. Development of the brain's default mode network from wakefulness to slow wave sleep. *Cereb. Cortex* 21, 2082–2093.
- Schabus, M., Dang-Vu, T.T., Heib, D.P.J., Boly, M., Desseilles, M., Vandewalle, G., Schmidt, C., Albouy, G., Darsaud, A., Gais, S., Degueldre, C., Balteau, E., Phillips, C., Luxen, A., Maquet, P., 2012. The fate of incoming stimuli during NREM sleep is determined by spindles and the phase of the slow oscillation. *Front. Neurosci.* 3, 40.
- Spoormaker, V.I., Schröter, M.S., Gleiser, P.M., Andrade, K.C., Dresler, M., Wehrle, R., Sämann, P., Czisch, M., 2010. Development of a large-scale functional brain network during human non-rapid eye movement sleep. *J. Neurosci.* 30, 11379–11387.
- Sporns, O., 2011. The non-random brain: efficiency, economy, and complex dynamics. *Front. Comput. Neurosci.* 5, 5.
- Sporns, O., Chialvo, D.R., Kaiser, M., Hilgetag, C.C., 2004. Organization, development and function of complex brain networks. *Trends Cogn. Sci.* 8, 418–425.
- Steinley, D., 2004. Properties of the Hubert-Arable adjusted Rand index. *Psychol. Methods* 9, 386–396.
- Stickgold, R., Malia, A., Maguire, D., Roddenberry, D., O'Connor, M., 2000. Replaying the game: hypnagogic images in normals and amnesics. *Science* 290, 350–353.
- Tagliazucchi, E., von Wegner, F., Morzelewski, A., Borisov, S., Jahnke, K., Laufs, H., 2012. Automatic sleep staging using fMRI functional connectivity data. *Neuroimage*. <http://dx.doi.org/10.1016/j.neuroimage.2012.06.036>.
- Tononi, G., 2004. An information integration theory of consciousness. *BMC Neurosci.* 5, 42.
- Tononi, G., 2005. Consciousness, information integration, and the brain. *Prog. Brain Res.* 150, 109–126.
- Tononi, G., Edelman, G.M., 1998. Consciousness and complexity. *Science* 282, 1846–1851.
- Tzourio-Mazoyer, N., Landeau, N., Papathanassiou, B., Crivello, D., Etard, O., Delcroix, N., Mazoyer, B., Joliot, M., 2002. Automated anatomical labeling of activations in SPM using a macroscopic anatomical parcellation of the MNI MRI single-subject brain. *Neuroimage* 15, 273–289.
- Vaessen, M.J., Braakman, H.M.H., Heerink, J.S., Jansen, J.F.A., Debeij-van Hall, M.H.J.A., Hofman, P.A.M., Aldenkamp, A.P., Backes, W.H., 2012. Abnormal modular organization of functional networks in cognitively impaired children with frontal lobe epilepsy. *Cereb. Cortex*. <http://dx.doi.org/10.1093/cercor/bhs186>.
- van den Heuvel, M.P., Stam, C.J., Boersma, M., Hulshoff Pol, H.E., 2008. Small-world and scale-free organization of voxel-based resting-state functional connectivity in the human brain. *Neuroimage* 43, 528–539.
- Wamsley, E.J., Perry, K., Djondragic, I., Babkes Reaven, L., Stickgold, R., 2010. Cognitive replay of visuomotor learning at sleep onset: temporal dynamics and relationship to task performance. *Sleep* 33, 59–68.